AIAA JOURNAL
Vol. 39, No. 9, September 2001

Modeling the Shapes of Constrained Partially Inflated High-Altitude Balloons

Frank Baginski* and William Collier†
George Washington University, Washington, D.C. 20052

During a balloon mission, the maximum film stresses most likely occur while the balloon is constrained by the launch spool. The focus is on shapes of very small gas volume that are representative of spool shapes and partially inflated ascent shapes where a launch collar is still attached. The balloon is constructed from long, flat, tapered sheets of 20.32-μm polyethylene that are sealed edge-to-edge to form a complete shape. Two caps are assumed to be located on top of the balloon. Load tapes are attached along the edges of the gores. The potential energy of the balloon system includes contributions due to hydrostatic pressure, film weight, load tape weight, film strain, and load tape strain. Solutions are determined that minimize the total energy subject to a volume constraint plus appropriate constraints to model nonfully deployed configurations. To model fine wrinkling in the balloon's membrane surface and to avoid compressive states, energy relaxation is employed. A number of numerical solutions are presented to illustrate the approach and provide estimates of the film stresses for these types of configurations.

Nomenclature

$\mathcal{C}_k$	=	class of piecewise differentiable surfaces with symmetry of the dihedral group D_k
D_k	=	dihedral group, the group of motions of the plane generated by rotations about the origin through an angle of $2\pi/k$ and reflections about some fixed axis
E	=	Young's modulus of balloon film
K_t	=	stiffness constant for load tape
N_F	=	number of facets in a triangulation of $\mathcal{S}_F$
n_c	=	number of circumferential fibers
n_g	=	number of gores in a complete balloon
$[R_d(s), 0, Z_d(s)]$	=	generating curve for design shape, where s is arc length, $0 \le s \le L_d$
$\mathcal{S}$	=	complete balloon surface
S_F	=	flat reference configuration corresponding to $\mathcal{S}_F$
$\mathcal{S}_F$	=	fundamental section of a balloon shape with a virtual fold
T_l	=	a facet in S_F
$\mathcal{T}_l$	=	a facet in $\mathcal{S}_F$
t	=	balloon film thickness
$\|u\|$	=	$\sqrt{(u_1^2 + u_2^2 + u_3^2)}$, where u is (u_1, u_2, u_3)
$\mathcal{V}$	=	volume of lifting gas enclosed by $\mathcal{S}$
W_f	=	standard membrane strain energy density
W_f^*	=	relaxed membrane strain energy density
W_t	=	standard load tape strain energy density
W_t^*	=	relaxed load tape strain energy density
w_f	=	gm_f weight density of balloon film
w_t	=	gm_t weight density of load tape
$\delta_{1,l}, \delta_{2,l}$	=	principal strains of facet T_l
$\mu_{1,l}, \mu_{2,l}$	=	principal stress resultants of facet T_l
ν	=	Poisson's ratio of balloon film

I. Introduction

TO design a more efficient high-altitude balloon, it is important to analyze their shapes at all stages of flight: launch, ascent, and float. Previous work on strained balloons considered cyclic shapes with volume $\mathcal{V}$ in the range $0.22 \cdot \mathcal{V}_d \le \mathcal{V} \le \mathcal{V}_d$, where $\mathcal{V}_d$ is the design volume, that is, the volume at float altitude.[1] However, because the maximum film stresses are most likely experienced while the balloon is constrained by the launch spool, it is important to give special attention to shapes of this type. In this paper, we will extend the results of Ref. 1 and consider constrained partially inflated configurations with significantly lower volumes (see Fig. 1). Shapes of this type are characterized by large-scale features such as folds of excess material and small-scale features such as fine wrinkling (see Fig. 2). Representations of these types of features are included in our model. For the solutions in Ref. 1, negative compressive stresses are present, but these are small in magnitude when compared to the meridional stresses and were ignored. However, when the gas bubble is very small ($\mathcal{V} \ll 0.01\mathcal{V}_d$), the compressive stresses are of higher magnitude and should not be ignored. With shapes of this type, the curvature of the balloon membrane is larger, and we interpret the higher compressive stresses as arising from fine wrinkling. For this reason, we use energy relaxation to model fine wrinkling and reformulate the problem in such a way that compressive stresses are avoided.[2] In addition, we will consider a number of constraints that are used to model nonfully deployed configurations of balloon shapes that are observed at launch (Fig. 1) or in early stages of ascent. Some of the results in this paper were announced by the first author in Ref. 3.

Membranelike structures have been studied previously (e.g., see Refs. 4 and 5). However, the situation for a typical large scientific balloon is much different. The film is extremely thin compared to the other membrane dimensions, and the differential pressure is comparatively small. These differences are discussed in more detail in Refs. 1–6. In addition, constraints of the type discussed here have not been considered elsewhere in the scientific literature.

The constraints that we consider are motivated by situations that arise in real balloons. After a large scientific balloon is launched, a collar is normally attached to the balloon. The collar prevents the portion of the balloon that lies below the gas bubble from deploying prematurely. The concern is that a gust of wind might turn the balloon into a giant sail. To model this situation, we assume that a band surrounds the balloon at a fixed distance above its base. This constraint (called a hoop constraint) prevents the circumferential fiber at that location from moving outside the band.

When the balloon is delivered to the launch site, it is folded in a certain fashion. Each gore is folded in half along its centerline, and the half-gores are stacked one on top of the other, with the half-gore at the top of the stack attached to the half-gore at the bottom of the stack. At launch, only the top 20% of the balloon is inflated. The remainder of the balloon lays on the ground (stacked as just described) and attached to the parachute and payload. A heavy cylinder (the launch spool) holds the partially inflated balloon in place (Fig. 1). The actual configuration of the balloon at launch is not axisymmetric, and it would be extremely difficult to model the way in which each individual gore is constrained by the launch

Received 3 July 2000; revision received 22 December 2000; accepted for publication 22 February 2001.

*Professor, Department of Mathematics; baginski@gwu.edu. Member AIAA.
†Graduate Student, Department of Mathematics; collier@gwu.edu.

Fig. 1 Spool configuration of large scientific balloon.

Fig. 2 Gore section of a partially inflated balloon showing a large-scale internal fold (center) and fine wrinkling.

spool. For this reason, we make some simplifying assumptions. In our model for the spool configuration, we assume that a hoop constraint (as earlier described) is applied and, in addition, the load tapes at this location are prevented from moving vertically. We will refer to a balloon shape constrained in this fashion as a spool-like configuration. These constraints are described in Secs. II and III.

In this paper, the design shape of the balloon is assumed to be known and based on the axisymmetric natural shape.[7] In the natural-shape model, it is assumed that the balloon membrane is inextensible and that the shape is in static equilibrium. The natural shape assumes that all of the tension is carried in the meridional direction and that the circumferential stress is zero. For our design shape, we use a variation of the natural shape that includes modifications due to cap and load tape weight.[8] In a real balloon, the film strains and hoop stresses are not necessarily zero. Near the top of the balloon, the film is under biaxial tension and behaves like a standard membrane. Below this region, the tension is predominantly in the meridional direction and the circumferential tension is negligible. Beginning with a fully inflated shape and then decreasing the size of the gas bubble, we see that the balloon envelope collapses, and the portion of the balloon that behaves like a standard membrane becomes smaller and concentrated near the top. The balloon film cannot support a compressive load, and so the film will wrinkle and form internal folds of excess material (Fig. 2). Following the work of Pipkin,[9] we approach the problem of membrane wrinkling by replacing the film strain energy density with its relaxation. We interpret a minimizer of the relaxed energy as an averaged representative of a wrinkled balloon membrane. Additional background on energy relaxation applied to large scientific balloons can be found in Ref. 10. Excess balloon film (a feature that is larger magnitude than the fine wrinkling) is represented through a virtual fold and is discussed Ref. 1. Because of the small gas volumes considered here, the relevant shapes will be such that most of the balloon will hang below the gas bubble, essentially in a state of uniaxial tension. It is important to estimate the distribution of folded material because its bulk will play a role in the formation of other large-scale features such as a lobe or a widow's peak. However, using an explicit fold without energy relaxation yields solutions with negative compressive stresses. For these reasons, we choose an approach that combines these two methods in our work.

II. Discrete Model for a Balloon Shape

An actual balloon is constructed from flat panels called gores that are heat-sealed edge-to-edge to form a complete closed shape. A discretized balloon shape is shown in Fig. 3. A balloon is assembled from multiple copies of a single gore. Viewed from above, Fig. 3 has the symmetries of a regular polygon with eight sides and so we say that the shape has D_8 symmetry. In general, a design shape with k gores will have D_k symmetry. In this paper, the number of gores will

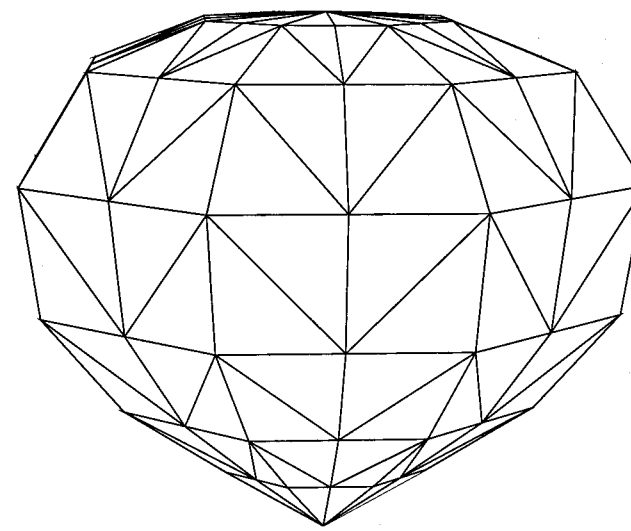

Fig. 3 Design shape assembled from eight gores with D_8 symmetry.

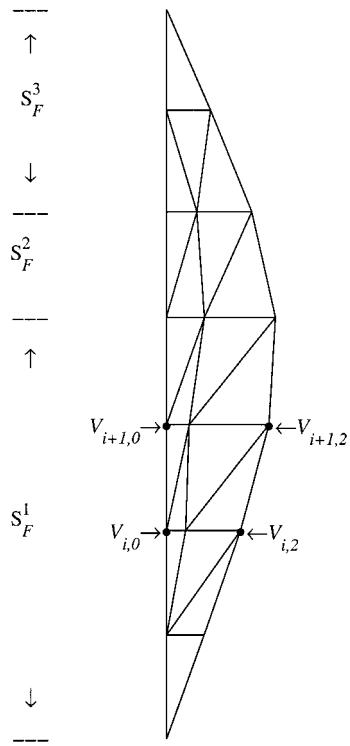

Fig. 4a S_F half-gore in the flat reference configuration.

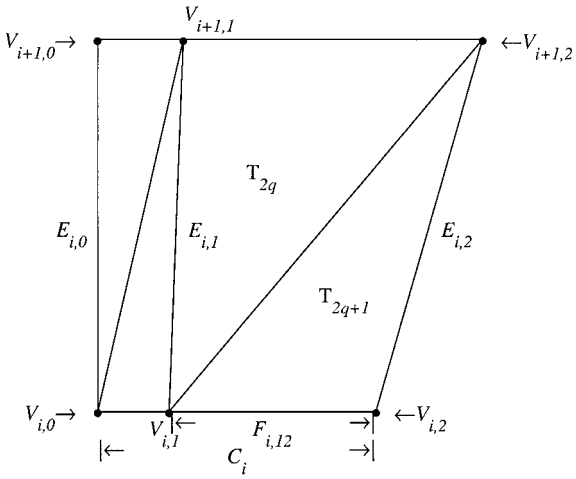

Fig. 4b Quadrilateral between meridional station i and $i+1$.

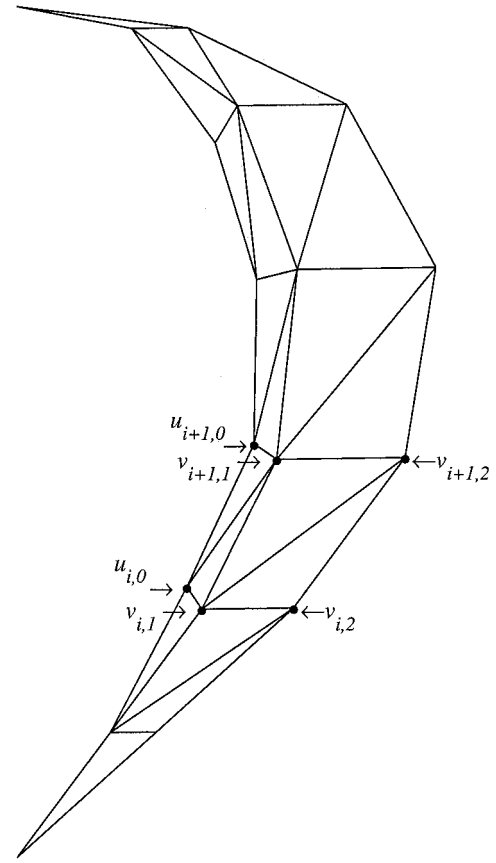

Fig. 5a S_F deformed half-gore with internal fold.

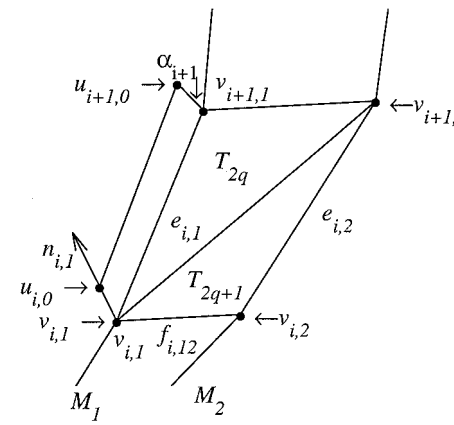

Fig. 5b Deformed quadrilateral between meridional station i and $i+1$; α_i is the length of the folded fiber at station i.

be denoted by n_g, that is, $k = n_g$. The class of all such balloon shapes is $\mathcal{C}_{n_g}$. A deformed gore is assumed to have a plane of reflectional symmetry, and so we need only to focus on a half-gore. A half-gore in the flat reference configuration is shown in Fig. 4. Later, we will describe in more detail how excess material is modeled.

We will adhere to the notation and conventions used in Ref. 1. For the convenience of the reader, we include a brief review of the mathematical model and include those aspects relevant to the hoop and spool-like constraints. As in Ref. 1, we model the complete balloon as a faceted surface with dihedral symmetry D_{n_g}. As such, the complete balloon can be modeled by a single half-gore. The base of the balloon lies at the origin of a Cartesian coordinate system. The central axis of the balloon shape lies along the z axis. The right-half gore lies in the region of R^3, where $0 \leq y \leq \tan(\pi/n_g)x$. We let $\mathcal{S}_F$ denote a fundamental section of the deformed balloon $\mathcal{S}$. We choose $\mathcal{S}_F$ to be the right half of a complete deformed gore that is centered about the xz plane. Excess material in $\mathcal{S}_F$ is tucked away in an internal fold lying in the xz plane. Reflecting $\mathcal{S}_F$ in the xz plane, we obtain its mirror image, which is denoted by $\mathcal{S}'_F$. Rotating $\mathcal{S}_F \cup \mathcal{S}'_F$ around the z axis n_g times in multiples of π/n_g, we can generate the complete balloon shape. There are three distinguished meridional fibers ($\mathcal{M}_0$, $\mathcal{M}_1$, and $\mathcal{M}_2$) that run along the length of the half-gore. $\mathcal{M}_2$ is a planar curve located in the $y = \tan(\pi/n_g)x$ plane and corresponds to the right edge of the deformed gore where the load tape is attached. Let $v_{i,2}$ be the vertices of $\mathcal{M}_2$. $\mathcal{M}_1$ with vertices $v_{i,1}$ is the fiber along the center of the deformed gore and lies in the xz plane. $\mathcal{M}_0$ (which will be described in more detail shortly) is the image in the deformed configuration of the fiber that runs along the center of the flat reference configuration (Fig. 4).

In Ref. 1, two methods of modeling excess balloon film are discussed. One method is referred to as an internal fold (Fig. 5). This model has the advantage of avoiding self-penetration for the complete shape and is consistent with the configuration of a real balloon that is partially inflated. This approach is acceptable for shapes near float where the amount of excess material is small.[6] However, bending the excess material into the xz plane has the effect of introducing fictitious stresses when the fold is not small. This problem can be avoided by the introduction of a relaxed strain energy

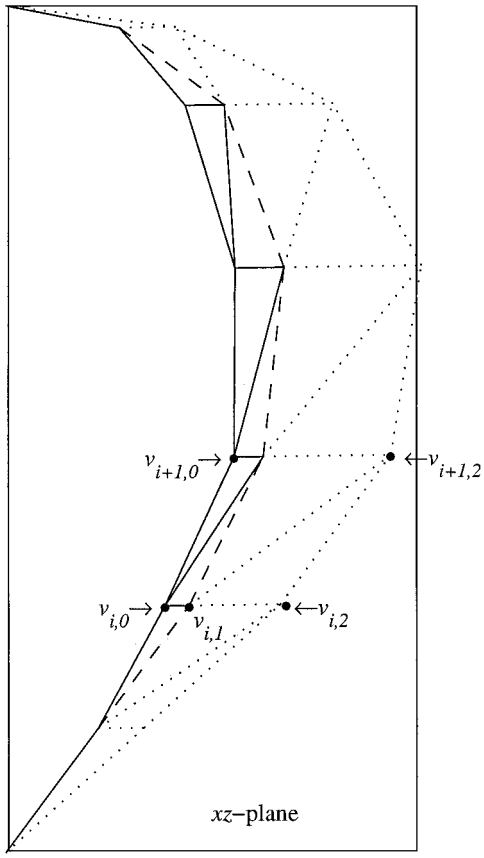

Fig. 6a S_F **deformed half-gore with virtual fold; triangles outlined in** $\cdots$ **lie in the region** $y > 0$.

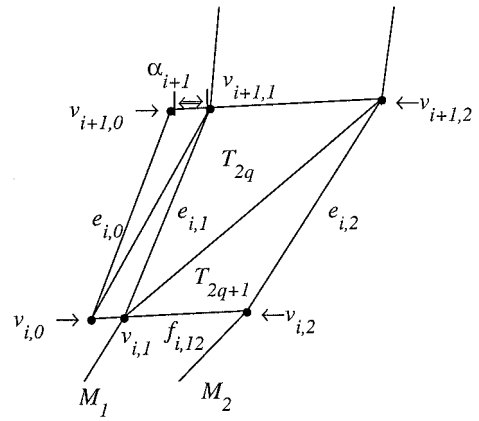

Fig. 6b Deformed quadrilateral between meridional station i **and** $i+1$; α_i **is the length of the folded fiber at station** i.

density.[2] Another method of modeling excess material that was implemented in Ref. 1 is a virtual fold. Figure 6 shows a deformed half-gore with a virtual fold. In a virtual fold, the fiber $\mathcal{M}_0$ can move into the region $y < 0$. Strictly speaking, the complete shape with a virtual fold will have self-penetration. However, the precise distribution of folded material is unknown, and the virtual fold leads to reasonable estimates of the film stresses.[1,2] Excess material is present at meridional station i if $v_{i,0} = (x_{i,0}, y_{i,0}, z_{i,0})$ and $y_{i,0} < 0$. Because this work will focus on balloon shapes with significant amounts of folded material, we will use the virtual fold method. In particular, $\mathcal{S}_F$ will denote a deformed half-gore with excess material represented by a virtual fold.

To each vertex $v_{i,j}$ in $\mathcal{S}_F$, there corresponds a vertex $V_{i,j}$ in the flat (undeformed) reference configuration S_F (Figs. 4 and 6). We define directed edges for meridional segments in $\mathcal{M}_j$ as

$$e_{i,j} = v_{i+1,j} - v_{i,j}, \qquad j = 0, 1, 2, \qquad i = 1, \ldots, n_c + 2 \tag{1}$$

In the reference configuration, the corresponding edges are

$$E_{i,j} = V_{i+1,j} - V_{i,j}, \qquad j = 0, 1, 2, \qquad i = 1, \ldots, n_c + 2 \tag{2}$$

We define the linear strain in the ith segment of $\mathcal{M}_j$ as

$$\varepsilon_{i,j} = (|e_{i,j}| - |E_{i,j}|)/|E_{i,j}| \tag{3}$$

For $i = 1, \ldots, n_c + 2$, we define circumferential fiber segments

$$c_i = v_{i,0} - v_{i,2} \tag{4}$$

$$f_{i,12} = v_{i,1} - v_{i,2} \tag{5}$$

$$C_i = V_{i,0} - V_{i,2} \tag{6}$$

$$F_{i,12} = V_{i,1} - V_{i,2} \tag{7}$$

The material points $V_{i,0}$ and $V_{i,2}$ remain fixed, and

$$V_{i,1} = V_{i,2} + (|f_{i,12}|/|c_i|)C_i \tag{8}$$

For each i, we see that the nodes $v_{i,0}$, $v_{i,1}$, and $v_{i,2}$ (as well as $V_{i,0}$, $V_{i,1}$, and $V_{i,2}$) are collinear. The shape $\mathcal{S}_F$ is a faceted surface, whose triangles are assembled as shown in Figs. 4 and 6:

$$\begin{aligned} &\mathcal{T}_l \in \mathcal{T}_F^o, \qquad \text{for} \qquad l = 1, \ldots, N_F^o \\ &\mathcal{T}_l \in \mathcal{T}_F^i, \qquad \text{for} \qquad l = N_F^o + 1, \ldots, N_F \end{aligned} \tag{9}$$

where $\mathcal{T}_F^o$ is the collection of triangles that form the outside of the fundamental section of a balloon, $\mathcal{T}_F^i$ is the collection of triangles that represent folded excess material, and $N_F = N_F^i + N_F^o$.

A typical balloon system will include external caps. For results presented here, the balloon has two caps that are modeled as an added thickness. Each layer is assumed to have the same material properties. To facilitate the mathematical description of caps, we partition the collection of facets S_F into three disjoint sets (Fig. 4), $S_F = S_F^1 \cup S_F^2 \cup S_F^3$. If a facet $T_l \in S_F^\tau$, then T_l has τ layers of film. The number of layers in $T_l \in S_F$ is defined by the function ω, where

$$\omega(T_l) = \tau, \qquad \text{for} \qquad T_l \in S_F^\tau, \qquad \tau \in \{1, 2, 3\} \tag{10}$$

Normally, vertices $v_{i,2} = (x_{i,2}, y_{i,2}, z_{i,2})$ $(i \neq 1, i \neq n_c + 2)$ have two degrees of freedom [because $y_{i,2} = \tan(\pi/n_g)x_{i,2}$], $v_{1,2} = (0, 0, 0)$ has zero degrees of freedom, and $v_{n_c+2,2} = (0, 0, z_{n_c+2,2})$ has one degree of freedom; $v_{i,1}$ is located at the point where the ith circumferential fiber penetrates the xz plane and is determined by $v_{i,0}$ and $v_{i,2}$. The balloon shape is a function of vertices in the form $v_{i,0}$, $v_{i,2}$.

If a hoop constraint is applied at station $i = i^*$, then we impose the condition

$$x_{i^*,1} \leq x_{i^*,1}^{\text{ub}} \tag{11}$$

For the complete shape, this essentially prevents the i^*th circumferential fiber from moving outside the band defined by Eq. (11). If a spool-like constraint is applied at station $i = i^*$, then

$$z_{i^*,2} = z_{i^*,2}^{\text{ub}} \tag{12}$$

is imposed simultaneously with Eq. (11). In the spool case, $v_{1,2} = (0, 0, z_{1,2})$ has one degree of freedom.

The design, that is, float, shape is a surface of revolution generated by a curve:

$$\gamma_d(s) = [R_d(s), 0, Z_d(s)], \qquad 0 \leq s \leq L_d \tag{13}$$

that is based on a variation of the natural shape, where the cap weight is modeled as an added thickness. This axisymmetric shape is discretized, and the complete discretized shape is assumed to be assembled from n_g identical copies of a single gore.

The total potential energy of a balloon configuration, E_{total}, is the sum of six terms:

$$E_{\text{total}} = E_{\text{gas}} + E_{\text{film}} + E_{\text{tape}} + E_{\text{top}} + S_{\text{tapes}} + S_{\text{film}} \tag{14}$$

where E_{gas} is the hydrostatic pressure potential due to the lifting gas, E_{film} is the gravitational potential energy of the film, E_{tape} is the gravitational potential energy of the load tapes, E_{top} is the gravitational potential energy of the top fitting, S_{tapes} is the strain energy of the load tapes, and S_{film} is the strain energy of the balloon film. These quantities are computed in the following manner.

A. Hydrostatic Pressure Potential

For a balloon at a fixed altitude, it is reasonable to assume that the densities of the lifting gas and ambient air (ρ_{gas} and ρ_{air}, respectively) are constant over the height of the balloon. In this case, the pressure difference across the balloon film at level z is given by

$$P = -g(\rho_{\text{air}} - \rho_{\text{gas}})(z - z_0) \tag{15}$$

where g is acceleration due to gravity and z_0 indicates the location of the zero-pressure level [e.g., see Ref. 11, Eq. (7), p. II.5]. The specific buoyancy at float will be denoted by $b_d = g(\rho_{\text{air}} - \rho_{\text{gas}})$, and b will denote the specific buoyancy at the current altitude. At float, we assume that $z_0 = 0$. The potential for hydrostatic pressure at float is

$$E_{\text{gas}} = -b_d \iiint_{\mathcal{V}} z \, \mathrm{d}V \tag{16}$$

where $\mathcal{V}$ is the region occupied by the gas bubble.[12] When the divergence theorem and the symmetries of $\mathcal{S}$ are used, Eq. (16) can be replaced by

$$E_{\text{gas}} = -2n_g b \sum_{l=1}^{N_F^o} \int_{\mathcal{T}_l} \frac{1}{2} z^2 \boldsymbol{k} \cdot \mathrm{d}\boldsymbol{A} \tag{17}$$

where $\mathrm{d}\boldsymbol{A} = \boldsymbol{n}\,\mathrm{d}A$, $\boldsymbol{n}$ is normal to $\mathcal{S}$, and $\mathrm{d}A$ is surface area measure on $\mathcal{S}$.

To reflect the denser atmosphere at a lower altitude corresponding to a volume $\mathcal{V} < \mathcal{V}_d$, the coefficient b_d in Eq. (16) is replaced by

$$b = b_d \mathcal{V}_d / \mathcal{V} \tag{18}$$

In this case, the pressure for an ascent shape is in the form

$$p(z) = bz + p_0$$

where p_0 is the Lagrange multiplier associated with the volume constraint. The zero-pressure level is given by $z_0 = p_0/b$ (see Ref. 10, p. 35).

B. Gravitational Potential Energy

The gravitational potential energy due to the weight of the balloon film (without caps) is

$$\int_{\mathcal{S}} w_f z \, \mathrm{d}S$$

where the film weight density is w_f. We will assume that one cap covers the top 29% of the balloon and a second covers the top 27%. Partitioning the collection of facets as described earlier and using the function ω [see Eq. (10)], we obtain the following approximation for E_{film} (including caps):

$$E_{\text{film}} = 2n_g w_f \sum_{l=1}^{N_F} \bar{z}_l \omega(T_l) \,\text{area}\,(T_l) \tag{19}$$

where $\bar{z}_l$ is the z component of the centroid of $\mathcal{T}_l$.

The gravitational potential energy due to load tape weight is

$$E_{\text{tape}} = n_g w_t \int_0^{L_d} \alpha_2(s) \cdot \boldsymbol{k} \, \mathrm{d}s$$

where w_t is the load tape weight density, $\alpha_2(s) \in R^3$ for $0 \le s \le L_d$ parametrizes $\mathcal{M}_2$, s is arc length in the flat reference configuration, and $\boldsymbol{k} = (0, 0, 1)$. The z component of the centroid corresponding to the edge $e_{i,2}$ is $\bar{z}_{i,2} = \frac{1}{2}(z_{i+1,2} + z_{i,2})$. The gravitational potential energy due to the load tapes in a complete shape is

$$E_{\text{tape}} = n_g w_t \sum_{i=1}^{n_c+1} \bar{z}_{i,2} |E_{i,2}| \tag{20}$$

C. Balloon Film Strain Energy

In what follows, we will assume that the balloon film is made up of a single layer. Using the function ω defined in the preceding section, we can add the contribution of the caps. The standard strain energy for the film is presented first and is followed by a development of the relaxed strain energy formulation. In our work, we use a standard measure of shell strain energy, for example, Eq. (1.1.20) of Ref. 13. However, because the balloon film has negligible bending stiffness, we drop terms related to the bending energy. When only the first integral in Eq. (1.1.20) of Ref. 13 is retained, the film strain energy S_{film} can be written in the form

$$S_{\text{film}} = \frac{1}{2} \int\int_{\Omega} W_f \, \mathrm{d}A^0 \tag{21}$$

where

$$W_f = n : \gamma \tag{22}$$

is the strain energy density function of the balloon film and Ω is the parameter space for the flat reference configuration. In Eq. (22), n is the second Piola–Kirchhoff stress tensor, γ is the Cauchy–Green strain tensor, and : is the tensor inner product. The contravariant components of n are $n^{\alpha\beta}$, the covariant components of γ are $\gamma_{\alpha\beta}$, and $n : \gamma = n^{\alpha}_{\beta} \gamma^{\beta}_{\alpha}$. Assuming a linear elastic istropic material, we have

$$n^{\alpha\beta} = E^{\alpha\beta\lambda\mu} \gamma_{\lambda\mu} \tag{23}$$

where $E^{\alpha\beta\lambda\mu}$ is the tensor of elastic moduli, that is,

$$E^{\alpha\beta\lambda\mu} = [tE/2(1+\nu)]\{a^{\alpha\lambda}a^{\beta\mu} + a^{\alpha\mu}a^{\beta\lambda} + [2\nu/(1-\nu)]a^{\alpha\beta}a^{\lambda\mu}\} \tag{24}$$

and

$$[a_{\alpha\beta}] = \begin{bmatrix} 1 & 0 \\ 0 & 1 \end{bmatrix}$$

is the first fundamental form of the flat reference configuration. We will compute the contribution to S_{film} for a typical facet, then sum the results to obtain an approximation of the total strain energy of $\mathcal{S}$.

Ultimately, we want to express the strain energy as a function of the nodes of the triangular facets. We first define all of the geometric and physical quantities for a typical facet. Let v_0^l, v_1^l, and v_2^l be the vertices of $\mathcal{T}_l$ and V_0^l, V_1^l, and V_2^l be the vertices of T_l. Let $M_{R,l}$ be the linear map that takes a standard triangle Ω^e with sides $\boldsymbol{i} = (1, 0)$, $\boldsymbol{j} = (0, 1)$ to $T_l \in S_F$, and let $M_{D,l}$ be the linear map that takes Ω^e to $\mathcal{T}_l \in \mathcal{S}_F$. The linear mappings $M_{R,l}$ and $M_{D,l}$ are represented by 2×2 and 3×2 matrices, respectively, where

$$M_{D,l} = \left[v_1^l - v_0^l \,\middle|\, v_2^l - v_1^l \right]$$

$$M_{R,l} = \left[V_1^l - V_0^l \,\middle|\, V_2^l - V_1^l \right]$$

Let $p \in T_l$ and $q \in \mathcal{T}_l$. The mapping $p \to q$ is given by

$$q = M_{D,l} M_{R,l}^{-1} p$$

The matrix $M_{D,l} M_{R,l}^{-1}$ is a linear mapping of p, and so the deformation gradient on facet l is

$$\boldsymbol{F}_l = \frac{\partial q}{\partial p} = M_{D,l} M_{R,l}^{-1}$$

In matrix form, the Cauchy strain is

$$\boldsymbol{C}_l = \boldsymbol{F}_l^T \boldsymbol{F}_l$$

and the Cauchy–Green strain γ is

$$\boldsymbol{G}_l = \tfrac{1}{2}(\boldsymbol{C}_l - \boldsymbol{I})$$

When an isotropic film and the linear stress–strain relation in Eq. (23) are assumed, the second Piola–Kirchhoff stress n in matrix form can be written as

$$\boldsymbol{S}_l = \lambda\left[\boldsymbol{G}_l + \nu \mathrm{Cof}(\boldsymbol{G}_l)^T\right] \tag{25}$$

where $\lambda = Et/(1-\nu^2)$ and the cofactor matrix of a 2×2 matrix is

$$\mathrm{cof}\left(\begin{bmatrix} a_{11} & a_{12} \\ a_{21} & a_{22} \end{bmatrix}\right) = \begin{bmatrix} a_{22} & -a_{12} \\ -a_{21} & a_{11} \end{bmatrix}$$

$\boldsymbol{G}_l$ and $\boldsymbol{S}_l$ are symmetric, and by the spectral representation, we have

$$\boldsymbol{G}_l = \delta_{1,l}\boldsymbol{n}_{1,l} \otimes \boldsymbol{n}_{1,l} + \delta_{2,l}\boldsymbol{n}_{2,l} \otimes \boldsymbol{n}_{2,l} \tag{26}$$

$$\boldsymbol{S}_l = \mu_{1,l}\boldsymbol{n}_{1,l} \otimes \boldsymbol{n}_{1,l} + \mu_{2,l}\boldsymbol{n}_{2,l} \otimes \boldsymbol{n}_{2,l} \tag{27}$$

where $\boldsymbol{n}_{1,l}$ and $\boldsymbol{n}_{2,l}$ are orthonormal vectors. The eigenvalues of $\boldsymbol{S}_l$ (denoted by $\mu_{1,l}$ and $\mu_{2,l}$) are the principal stress resultants[14] and the eigenvalues of $\boldsymbol{G}_l$ (denoted by $\delta_{1,l}$ and $\delta_{2,l}$) are principal strains. Because we have assumed a linear and isotropic relationship between the stress and strain, $\boldsymbol{S}_l$ and $\boldsymbol{G}_l$ have the same principle axes.

The film strain density on triangle T_l is given by

$$W_f(T_l) = \boldsymbol{S}_l : \boldsymbol{G}_l \tag{28}$$

Because n and γ are constant on each T_l in a constant strain model, we can approximate Eq. (21) by

$$2n_g \sum_{l=1}^{N_F} \frac{1}{2} W_f(T_l) \int_{T_l} \mathrm{d}A^0 \tag{29}$$

After adding the contribution of the external caps, the film strain energy can be approximated by

$$S_{\mathrm{film}} = 2n_g \sum_{l=1}^{N_F} \frac{1}{2} \omega(T_l) W_f(T_l)\, \mathrm{area}(T_l) \tag{30}$$

In the following, we will refer to Eq. (30) as the standard membrane energy of the balloon.

When dealing with the relaxed energy, it will be convenient to have an expression for W_f in terms of the principal strains in a typical facet T_l, that is,

$$W_f(T_l) = [E/2(1-\nu^2)]\left(\delta_{1,l}^2 + \delta_{2,l}^2 + 2\nu\delta_{1,l}\delta_{2,l}\right) \tag{31}$$

Remark: When using the standard membrane energy of the balloon, it is much more efficient to use Eq. (28) instead of Eq. (31) because Eq. (31) requires solving an eigenvalue problem to determine the principal strains to evaluate W_f.

The energy density in Eq. (31) can lead to states where $\mu_{1,l}$ or $\mu_{2,l}$ are negative, corresponding to a compression. However, the balloon film cannot support such a compression and will actually fold or wrinkle instead. To tackle the problem of negative compressive stresses in the solution, we follow the methods introduced by Pipkin.[9] The methods of Pipkin were adapted to large scientific balloons by the second author in Refs. 2 and 10. To simplify the notation for the general discussion that follows, we temporarily drop the subscript l. Let δ_1 and δ_2 be the principal (Cauchy–Green) strains for a typical facet. Let μ_1 and μ_2 be the corresponding principal stress resultants.

In Pipkin's approach,[9] a membrane M is decomposed into three distinct regions: S slack region, where the Cauchy–Green strains are both negative, that is, $\delta_1 < 0$, $\delta_2 < 0$; T tense region, where both principal stress resultants are positive, that is, $\mu_1 > 0$, $\mu_2 > 0$; and U wrinkled region ($U = M \backslash S \cup T$).

We apply this classification scheme to each $\mathcal{T}_l$ in our triangulation of $\mathcal{S}_F$.

On S the strain energy is assumed to be zero and on T the relaxed strain energy density is exactly the same as the standard strain energy density [see Eq. (31)]. On the region U, we use a modified Cauchy–Green strain $\boldsymbol{G}^*$. If $\boldsymbol{G}$ is the usual Cauchy–Green strain, then

$$\boldsymbol{G}^* = \boldsymbol{G} + \beta^2 \boldsymbol{n} \otimes \boldsymbol{n} \tag{32}$$

where $\boldsymbol{n}$ and $\boldsymbol{t}$ are (unknown) principal stress directions based on $\boldsymbol{G}^*$. Pipkin[9] refers to $-\beta^2 \boldsymbol{n} \otimes \boldsymbol{n}$ as the wrinkling strain and $\boldsymbol{G}^*$ as the elastic strain. The elastic strain is thought to represent the straining in an averaged wrinkled surface and leads to uniaxial stress on U in the form

$$\boldsymbol{S}^* = \mu \boldsymbol{t} \otimes \boldsymbol{t} \tag{33}$$

where $\mu > 0$ and $\boldsymbol{t}$ is a unit vector orthogonal to $\boldsymbol{n}$. For our discussion, we assume that $\boldsymbol{t}$ is the tensile direction, and $\boldsymbol{n}$ is a unit vector orthogonal to $\boldsymbol{t}$. The parameter β^2 and $\boldsymbol{n}$ are chosen in such a way that the following conditions are satisfied:

$$\boldsymbol{n} \cdot \boldsymbol{S}^* \boldsymbol{n} = 0 \tag{34}$$

$$\boldsymbol{n} \cdot \boldsymbol{S}^* \boldsymbol{t} = 0 \tag{35}$$

For an isotropic material, $\boldsymbol{S}^*$ can be written in the form

$$\boldsymbol{S}^* = \boldsymbol{S} + \beta^2 \boldsymbol{K}$$

where

$$\boldsymbol{K} = \lambda[\boldsymbol{n} \otimes \boldsymbol{n} + 2\nu\, \mathrm{cof}(\boldsymbol{n} \otimes \boldsymbol{n})^T]$$

It follows that, for an isotropic material,

$$\beta^2 = -(1/\lambda)\boldsymbol{n} \cdot \boldsymbol{S}\boldsymbol{n} \tag{36}$$

If $W_f(\boldsymbol{G})$ is the standard strain energy density function, the relaxed strain energy density is $W_f(\boldsymbol{G}^*)$, where $\boldsymbol{G}^*$ uses β^2 from Eq. (36) and $\boldsymbol{n}$ is the principal direction that corresponds to a positive principal strain.

The large-scale folds are taken into account by the set $\mathcal{T}_F^i$. The wrinkling behavior is taken into account by replacing the standard energy density W_f by its relaxation W_f^*. Because W_f^* is constant on each T_l, we have

$$W_f^*(T_l) = \begin{cases} 0 : \delta_{1,l} < 0, & \delta_{2,l} < 0 \\ \tfrac{1}{2}E\delta_{1,l}^2 : \mu_{1,l} \le 0, & \delta_{2,l} \ge 0 \\ \tfrac{1}{2}E\delta_{2,l}^2 : \mu_{2,l} \le 0, & \delta_{1,l} \ge 0 \\ [E/2(1-\nu^2)]\left(\delta_{1,l}^2 + \delta_{2,l}^2 + 2\nu\delta_{1,l}\delta_{2,l}\right) : \mu_{1,l} \ge 0, & \mu_{2,l} \ge 0 \end{cases} \tag{37}$$

If the strain energy density in Eq. (21) for the deformed surface is replaced by its relaxation, we have

$$S_{\mathrm{film}}^* = \frac{1}{2} \int\int_{\Omega} W_f^* \, \mathrm{d}A^0 \tag{38}$$

Adding the contribution of the external caps, we find that Eq. (38) can be approximated by

$$S_{\mathrm{film}}^* = 2n_g \sum_{l=1}^{N_F} \frac{1}{2} \omega(T_l) W_f^*(T_l)\, \mathrm{area}(T_l) \tag{39}$$

The standard membrane energy of the balloon is given by Eq. (30), whereas its relaxed energy is given by Eq. (39).

D. Load Tape Strain Energy

We assume that a fiber segment in a load tape behaves like a linearly elastic string with stiffness constant K_t. The tape strain in a segment is given by Eq. (3). The value for K_t is determined experimentally and has the units of force. If we denote the strain energy density of the load tape by

$$W_t(\varepsilon) = \tfrac{1}{2}K_t\varepsilon^2$$

where ε is the strain, then the total strain energy of the load tapes in a complete shape is

$$S_{\text{tapes}} = n_g \sum_{i=1}^{n_c+1} W_t(\varepsilon_{i,2})|E_{i,2}| \tag{40}$$

The convexification of the strain energy density for the load tape is given by

$$W_t^*(\varepsilon) = \begin{cases} W_t(\varepsilon), & \epsilon \geq 0 \\ 0, & \epsilon < 0 \end{cases}$$

When the relaxed energy is used for the load tapes, the total strain energy of the load tapes is

$$S_{\text{tapes}}^* = n_g \sum_{i=1}^{n_c+1} W_t^*(\varepsilon_{i,2})|E_{i,2}| \tag{41}$$

See Ref. 10 for a further discussion on the convexification of the load tape strain energy density.

E. Variational Principle

The discrete form of the total energy of $\mathcal{S}$ with the standard membrane and load tape strain energies will be denoted by $E(v_{i,j})$ and is obtained by substituting Eqs. (17), (19), (20), (30), and (40) into Eq. (14). The term $E_{\text{top}} = w_{\text{top}} z_{\text{top}}$ in Eq. (14) is the gravitational potential due to the weight of the top fitting and $z_{\text{top}} = z_{2,n_c+2}$ is its height above the base of the balloon. The discrete form of the total energy of $\mathcal{S}$ with relaxed strain energies is given by $E^*(v_{i,j})$ and is obtained using Eqs. (17), (19), (20), (39), and (41).

The gas bubble is partitioned into tetrahedra, all of which have a common vertex located on the z axis inside the gas bubble. The lth tetrahedron has facet $\mathcal{T}_l$ as its base, and its volume is denoted by $\mathcal{V}_l$. The total volume of the gas bubble $\mathcal{V}$ is constrained so that

$$\mathcal{V} - 2n_g \sum_{l=1}^{N_F^o} \mathcal{V}_l = 0 \tag{42}$$

Upper and lower bounds in the form

$$\begin{aligned} v_{i,0}^{\text{lb}} \leq v_{i,0} \leq v_{i,0}^{\text{ub}}, \qquad & i = 2, \ldots, n_c + 1 \\ v_{i,2}^{\text{lb}} \leq v_{i,2} \leq v_{i,2}^{\text{ub}}, \qquad & i = 2, \ldots, n_c + 1 \end{aligned} \tag{43}$$

are imposed. Bounds in Eq. (43) are applied only to free parameters. The upper and lower bounds are chosen sufficiently large so they do not affect the solution (except when they are being used to represent a specific constraint). The variational principle that is used to compute a balloon shape is

$$\begin{array}{lll} & \text{Problem}(\star) & \\ \text{for } \mathcal{S}(v_{i,j}) \in \mathcal{C}_k, & \text{minimize:} & E(v_{i,j}) \\ & \text{subject to:} & \boldsymbol{G}(v_{i,j}) \leq 0 \end{array}$$

satisfying Eq. (43), where the first component of $\boldsymbol{G} \leq 0$ is defined by the equality constraint Eq. (42). A solution of problem ($\star$) is called an energy minimizing shape (EM shape). If a circumferential constraint is to be imposed at station i^*, then Eq. (11) is included as a linear inequality constraint in $\boldsymbol{G}$. To model the vertical constraint for a spool-like configuration, we impose Eq. (12) by modifying Eq. (43) appropriately. MATLAB® software (constr) is used to solve problem ($\star$). If energy relaxation is applied to the film and load tape strain energies, then $E^*(v_{i,j})$ is used in place of $E(v_{i,j})$.

III. Numerical Solutions

For our calculations, we consider a 832,062-m^3 two-cap balloon. The balloon film is 20.32-μm polyethylene. We use a specific buoyancy that corresponds to a float altitude of 40,600 m (see Ref. 15, p. 73). Our values for material constants such as Poisson's ratio ν, Young's modulus E, and load tape stiffness K_t are appropriate for float conditions of a typical scientific balloon.[16] The payload is adjusted so that the balloon is in equilibrium at float. In this paper, the payload includes the weight of the scientific instruments, venting ducts, fins, inflation tubes, backup tapes, etc. For our design shape, the payload is 10.5156 kN, the top fitting weighs 0.1334 kN, and the total weight of the balloon system is 24.6253 kN. See Table 1 for additional parameter values. For most of our results, the number of circumferential fibers used in our model is $n_c = 19$. At the start, the meridional segments are of equal length. As the gas bubble becomes smaller, we choose a denser mesh near the top of the balloon where the gas bubble forms and use a coarser mesh in the lower portion of the balloon. For the spool case, we used meshes with $n_c = 19$ and $n_c = 33$.

Table 1 Parameter values

Description (unit)	Variable	Value
Young's modulus (MPa)	E	248.211
Poisson's ratio	ν	0.82
Film mass density (g/m^2)	m_f	18.7485
Load tape mass density (g/m)	m_t	10.6552
Load tape stiffness parameter (kN)	K_t	26.2445
Film thickness (μm)	t	20.32
Specific buoyancy at float (N/m^3)	b_d	0.0295389
Specific buoyancy at launch (N/m^3)	b_0	8.87089
Volume at float (m^3)	$\mathcal{V}_{\text{float}}$	832,062
Number of gores	n_g	159
Design gore length (m)	ℓ_d	180.668

Table 2 Strained EM shapes at float with and without energy relaxation[a]

Quantity	Design	Standard	Relaxed
E_{total}	−561.6070	−571.8208	571.8893
E_{gas}	−1464.03	−1502.37	−1502.78
E_{film}	716.0827	730.4785	730.8478
E_{tape}	172.6392	176.3707	176.4407
E_{top}	13.7063	14.0567	14.0658
S_{film}	0	3.2899	3.2663
S_{tapes}	0	6.3584	6.2736
$(\min \varepsilon_{i,0}, \max \varepsilon_{i,0})$	(0.0, 0.0)	(0.0015, 0.0055)	(0.0024, 0.0054)
$(\min \varepsilon_{i,1}, \max \varepsilon_{i,1})$	(0.0, 0.0)	(0.0015, 0.0055)	(0.0015, 0.0055)
$(\min \varepsilon_{i,2}, \max \varepsilon_{i,2})$	(0.0, 0.0)	(0.0015, 0.0054)	(0.0015, 0.0054)
$\theta_{1,1}$ (deg)	57.460	61.475	61.52
z_{top}	102.7095	105.3358	105.403
$\max_i x_{i,1}$	64.3501	64.0931	64.0276
$\max_i \mu_{i,1}$ (N/cm)	0	1.35264	1.36581
$\max_i \mu_{i,2}$ (N/cm)	0	1.3694	1.38501
z_0	0	1.917	0.029972

[a]Units: length, m; force, N; and energy, kJ.

We are interested in shapes with volumes that are significantly less than the volume at float. To determine these shapes, we begin by evolving the discrete unstrained design shape to its equilibrium [as defined by problem ($\star$)]. We find that there is essentially no excess material in the strained float shape. Solutions obtained by using the standard and relaxed energies are presented in Table 2. The parameter $\theta_{i,1}$ denotes the angle the tangent to $\mathcal{M}_1$ makes with the z axis at station i ($2\theta_{1,1}$ is the angle at the base of the balloon). Because W_f^* requires the calculation of the principal strains and principal stresses, the evolution of a relaxed EM shape is more time consuming than the evolution of a standard EM shape. For this reason, we first calculate a family of EM shapes using the ordinary membrane energy. The solution based on the standard membrane energy is used as the initial guess for the relaxed EM shape of interest.

Beginning with the strained float shape, we decrement the volume and compute the corresponding EM shape, continuing until $\mathcal{V} = 0.005\mathcal{V}_d$. Initially, we must take extremely small steps, or else the solution process will diverge. We choose $\triangle\mathcal{V} \approx 0.0001\mathcal{V}_d$, until $\mathcal{V} \approx 0.97\mathcal{V}_d$. After we have computed an EM shape with $\mathcal{V} = 0.97\mathcal{V}_d$, larger steps can be taken. If $(\mathcal{V}_k, \mathcal{S}_k)$ is the volume and corresponding EM shape at the start, we use $(\mathcal{V}_k, \mathcal{S}_k)$ as the initial guess for the solution $(\mathcal{V}_{k+1}, \mathcal{S}_{k+1})$, where $\mathcal{V}_{k+1} = \mathcal{V}_k - \triangle\mathcal{V}$. We found that the size of the volume decrement could be increased if we used linear interpolation between pairs $(\mathcal{V}_{k-1}, \mathcal{S}_{k-1})$ and $(\mathcal{V}_k, \mathcal{S}_k)$ to predict

Table 3 Strained EM shapes at $\mathcal{V}$= 0.005 $\mathcal{V}_d$ with and without energy relaxation[a]

	No hoop constraint		Hoop constraint	
Quantity	Standard energy	Relaxed energy	Standard energy	Relaxed energy
E_{total}	−2568.60	−2579.56	−2566.58	−2577.5
E_{gas}	−3973.82	−3984.51	−3971.30	−3981.77
E_{film}	1109.51	1109.45	1109.07	1108.88
E_{tape}	268.0057	267.9993	267.8381	267.7986
E_{top}	22.8939	22.8909	22.8357	22.8307
S_{film}	1.7104	1.4832	1.7686	1.7252
S_{tapes}	3.0751	3.0858	3.2109	3.0281
$(\min \varepsilon_{i,0}, \max \varepsilon_{i,0})$	(0.0015, 0.0055)	(0.0008, 0.0083)	(0.0024, 0.0058)	(0.0009, 0.0110)
$(\min \varepsilon_{i,1}, \max \varepsilon_{i,1})$	(0.0023, 0.0054)	(0.0023, 0.0081)	(0.0023, 0.0058)	(0.0022, 0.0110)
$(\min \varepsilon_{i,2}, \max \varepsilon_{i,2})$	(0.0023, 0.0047)	(0.0023, 0.0045)	(0.0023, 0.0049)	(0.0022, 0.0048)
$\theta_{1,1}$ (deg)	0.305	0.0653	0.305	0.0653
z_{top}	171.5582	171.5361	171.1221	171.0845
$\max_i x_{i,1}$	9.9110	9.9515	10.0333	10.0927
Constraint $x_{i^*,1}$	1.8062	1.8247	1.1176	1.1176
Constraint $\theta_{i^*,1}$ (deg)	22.11	22.26	27.81	28.20
$\max_i \mu_{i,1}$ (N/cm)	3.18941	3.21182	3.39798	3.4493
$\max_i \mu_{i,2}$ (N/cm)	3.25088	3.27032	3.47522	3.51024
z_0	156.2626	156.4142	155.2705	155.1889

[a]Units: length, m; force, N; and energy, kJ.

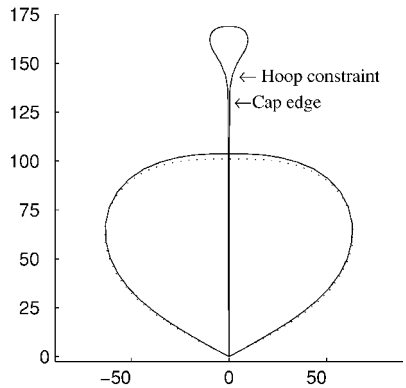

Fig. 7a Design shape and strained float shape (· · · ·, design, and ——, strained float); ascent shape at $\mathcal{V}$= 0.005 $\mathcal{V}_d$.

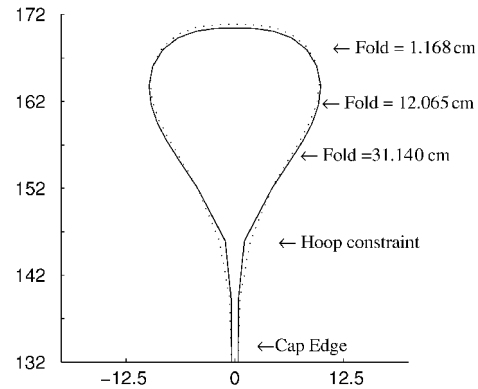

Fig. 7b Top portion of ascent shape at $\mathcal{V}$= 0.005 $\mathcal{V}_d$ with depth of internal fold (· · · ·, without hoop constraint, and ——, with hoop constraint); units: length, in.

the initial shape for $\mathcal{V} = \mathcal{V}_{k+1}$. In this case, steps on the order of $\triangle\mathcal{V} \approx 0.005\mathcal{V}_d$ could be achieved. This process was continued until we computed the solution for $\mathcal{V} = 0.005\mathcal{V}_d$. As we approached $\mathcal{V} = 0.005\mathcal{V}_d$, smaller volume decrements were used. Data on the EM shapes with $\mathcal{V} = 0.005\mathcal{V}_d$ with and without energy relaxation are presented in Table 3. We then imposed the hoop constraint and computed a family of EM shapes with decreasing hoop constraint diameter. In particular, when $\mathcal{V} = 0.005\mathcal{V}_d$, we found that at station $i^* = 9$, $x_{i^*,1} = 1.80619$ m. We set $x^{\text{ub}}_{i^*,1} = 1.8034$ and computed an EM shape with the additional hoop constraint. With the volume fixed, we then continued to decrement $x^{\text{ub}}_{i^*,1}$ (in steps of roughly 5 cm), until $x^{\text{ub}}_{i^*,1} = 1.1176$. The results for $x^{\text{ub}}_{i^*,1} = 1.1176$ are summarized in Table 3.

In Fig. 7a, we present the design shape, the strained design shape at float, and the ascent shape at $\mathcal{V} = 0.005\mathcal{V}_d$. The location of the caps and hoop constraints are indicated. In Fig. 7b, we present a close-up of the top portion of the ascent shape. The amount of excess material (represented by the depth of the fold) at various locations is also presented in Fig. 7b. Because of the coarseness of our model, a 2.5-cm fold is negligible.

To obtain single measurements for the principal stress resultants for a quadrilateral formed from two adjacent triangles $T_{2q} \cup T_{2q+1}$, the values of the respective resultants are averaged. The averaged stress resultants give a rough measure of the deformation at each meridional station. In Figs. 8a and 8b, we present the averaged principal stress resultants for shapes presented in Tables 2 and 3. The minimum principal stress resultant for the strained design shape using the standard film strain energy is −0.079 N/cm. After relaxation, this value is 0, and there is a 1% increase in the maximum principal stress resultants. Because they are essentially the same, only results based on the standard strain energy are plotted in Fig. 8.

Note that when the gas bubble has decreased from $\mathcal{V}_d$ to $0.005\mathcal{V}_d$, the maximum principal stresses are more than doubled (see max $\mu_{i,j}$ in Table 3). In Fig. 8c, we present the tension in the load tapes for the shapes presented in Tables 2 and 3. At float, the maximum load tape tension occurs near the bottom of the balloon. It is at float that the angle at the base of the balloon is largest (and so the reaction force due to the payload is largest). As the volume decreases, this angle decreases along with the tension in the load tape in the lower portion of the balloon. As the volume decreases, we observe a slight increase in the maximum load tape tension, but we also observe that the load tape near the top of the balloon (for small volumes) works to carry more of the weight of the balloon system [note the increase in the minimum load tape strain $\min(\varepsilon_{2,j})$ in Table 3]. Even though the caps were added to reinforce the balloon while constrained by the launch spool, our results show that they serve a useful purpose during ascent (long after release from the spool). For the example presented here, if we assume that the volume of the balloon at launch is $0.0033\mathcal{V}_d$, then an increase to $\mathcal{V} = 0.005\mathcal{V}_d$ would correspond to an increase in altitude of nearly 3048 m.

To compute the spool-like configuration, we used the earlier computed ascent shape solution with hoop constraint and added a vertical constraint by fixing $z_{i^*,2} = 144.27$ m. At launch, we assume $\mathcal{V} = 0.0033\mathcal{V}_d$. By Eq. (18), we find that the corresponding buoyancy b_0 is

$$b_0 = (\mathcal{V}_d/\mathcal{V})b_d = 303.03b_d$$

We decrement the volume and hoop constraint (sometimes simultaneously) until we computed an EM shape with $x_{i^*,1} = 0.66$ m and $\mathcal{V} = 0.0033\mathcal{V}_d$. Data on this spool-like configuration are presented in Table 4. To reach float altitude more efficiently, additional lifting

Table 4 Spool-like EM shapes; $\mathcal{V}$= 0.0033 $\mathcal{V}_d$ with and without energy relaxation[a]

	Standard energy		Relaxed energy	
Quantity	$n_c = 19$	$n_c = 33$	$n_c = 19$	$n_c = 33$
E_{total}	−2616.91	−2624.59	−2634.81	−2635.35
E_{gas}	−4022.19	−4040.92	−4040.16	−4040.93
E_{film}	1109.89	1110.28	1109.85	1110.29
E_{tape}	268.18	268.21	268.19	268.22
E_{top}	23.0377	23.0309	23.0374	23.0302
S_{film}	1.6397	12.0788	1.6612	1.3139
S_{tapes}	2.9002	3.0860	2.9973	3.0762
(min $\varepsilon_{i,0}$, max $\varepsilon_{i,0}$)	(0.0023,0.0053)	(0.0024, 0.0051)	(0.0010, 0.0122)	(0.0024, 0.0051)
(min $\varepsilon_{i,1}$, max $\varepsilon_{i,1}$)	(0.0022,0.0052)	(0.0022, 0.0051)	(0.0022, 0.0122)	(0.0020, 0.0051)
(min $\varepsilon_{i,2}$, max $\varepsilon_{i,2}$)	(0.0022,0.0046)	(0.0022, 0.0051)	(0.0022, 0.0047)	(0.0022, 0.0051)
$\theta_{1,1}$ (deg)	0.305	0.065	0.065	0.065
z_{top}	6796.68	6794.67	6796.59	6794.47
z_{bot}	−1.377	−1.341	−1.447	−1.267
$\max_i x_{i,1}$	8.6279	8.6284	8.6670	8.6330
Constraint $\theta_{i^*,1}$ (deg)	13.92	11.4549	14.79	11.4257
$\max_i \mu_{i,1}$ (N/cm)	3.3563	3.38905	3.52618	3.40411
$\max_i \mu_{i,2}$ (N/cm)	3.41725	3.39186	3.63003	3.40429
z_0	159.3007	159.1841	159.1917	159.1841

[a]Units: length, m; force, N; and energy, kJ.

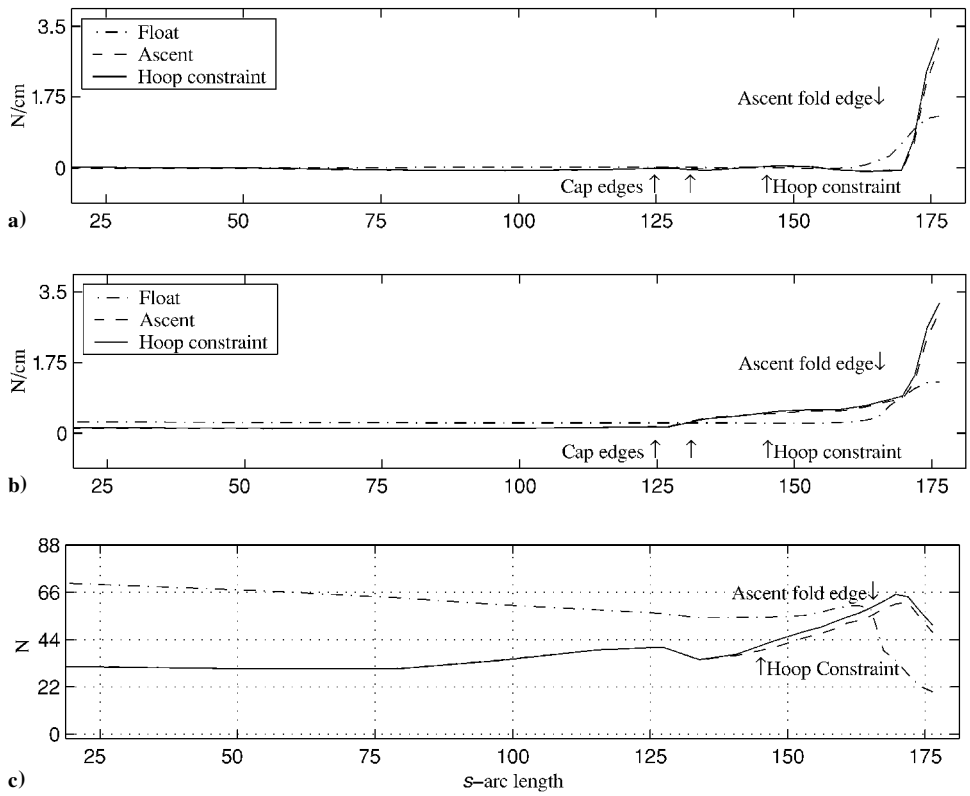

Fig. 8 EM shapes with $\mathcal{V}$= $\mathcal{V}_d$, $\mathcal{V}$= 0.005 $\mathcal{V}_d$ without hoop constraint, and $\mathcal{V}$= 0.005 $\mathcal{V}_d$ with hoop constraint: a) circumferential stress resultants, b) meridional stress resultants, and c) load tape tension where *s* is distance from base (in.).

gas is injected into the balloon at launch. (The excess gas is vented before reaching float.) To simulate this, one can increase the buoyancy constant by 10–15% (while keeping the volume fixed). The net effect is that the hydrostatic pressure increases proportionally. Accordingly, the maximum principal stress resultants increase by 10–15% (Ref. 3).

In Figs. 9a and 9b, we present the averaged principal stress resultants for a spool-like configuration using the relaxed energy. As one would expect, for a pair of adjacent triangles T_{2q} and T_{2q+1}, the facet near the center, T_{2q}, is usually more strained than a facet with a load tape edge (T_{2q+1}). The variation between T_{2q} and T_{2q+1} is more noticeable in the top portion of the balloon, where the membrane is under biaxial tension. The actual spool constraint for our design would be imposed closer to the bottom of the balloon, so the maximum film stresses would be slightly lower than those reported in Table 4.

Because of the higher principal curvatures in a spool configuration, we observe features in our solutions that are not present in EM shapes with $0.01\mathcal{V}_d < \mathcal{V} < \mathcal{V}_d$. In the spool configuration, a local peak in the meridional stress resultant is noticeable where the balloon's radius is a maximum (near $s = 167.64$). In his analysis of data from a real partially inflated balloon Winker[17] noted a drop in the load tape tension in this region (which must be accompanied by an increase in film tension). The meridional stress resultant is decreasing on the interval $167.64 < s < 174$ and takes on a local minimum at $s = 174$. The load tape tension is increasing for $167.64 < s < 174$ and reaches a local maximum at $s = 174$. Near $s = 174$, the state of the membrane changes from uniaxial to a biaxial. A similar behavior

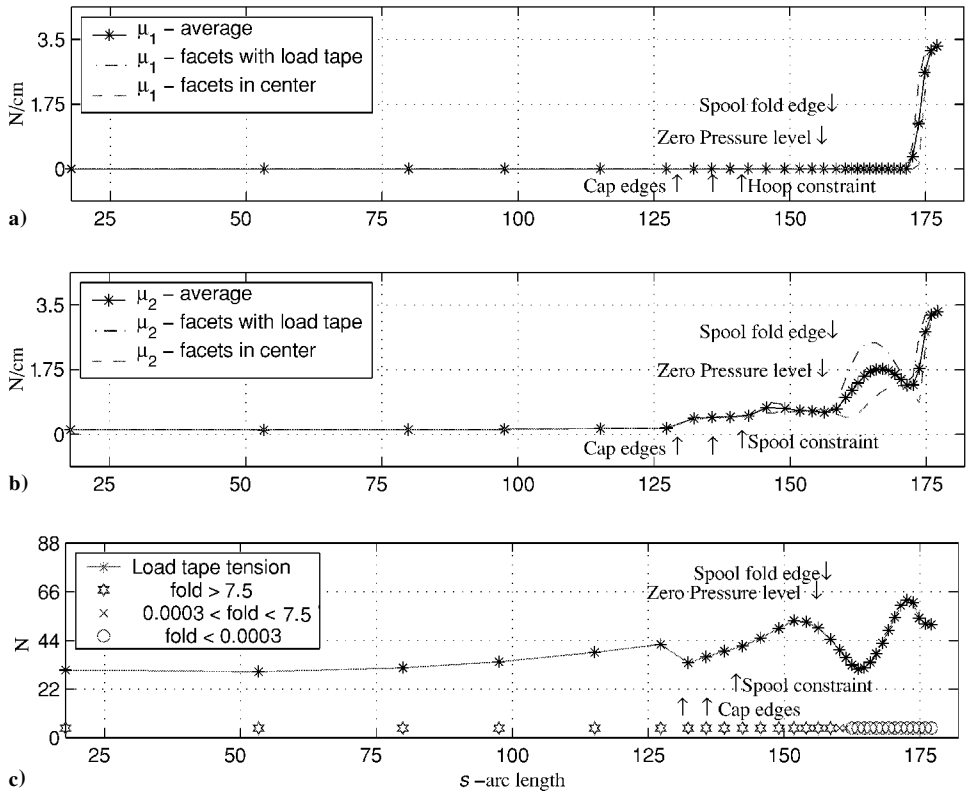

Fig. 9 Averaged stress resultants for spool-like shape: a) hoop, b) meridional, and c) load tape tension for spool-like shapes where s is distance from base.

was observed for small volumes, for example $\mathcal{V} = 0.01\mathcal{V}_d$, independent of the spool constraint, but this effect is more noticeable when $\mathcal{V} \ll 0.01\mathcal{V}_d$. We also note that for the spool shape presented in Table 4 and Fig. 9, the principal directions deviate slightly from what we call the meridional and circumferential directions. However, this deviation is not the cause of the local peak in the meridional stress resultant.

There are characteristics of nonaxisymmetric spool shapes that are not represented in our present half-gore model. Near the top of the balloon in the center of Fig. 1, we observe a protrusion that is sometimes called a widow's peak. Although it is not evident from the photograph, in the vicinity of the top of balloon, both principal curvatures of the membrane are positive, and the shape is without protrusions. Symmetry breaking with the appearance of a widow's peak could be due to the constraining device. However, even if the balloon could be constrained in a symmetric fashion (as in our spool-like model), it is likely the same type of protrusion would be observed. A widow's peak is due to the overabundance of excess film and the presence of meridional fiber segments that are longer than normal (see Fig. 7a). We conjecture that the symmetric shape generated by the half-gore model is unstable, and a shape of the type shown in Fig. 1 is stable. However, although a shape as in Fig. 1 may have some high stresses in certain concentrated regions, the principal stress resultants obtained from the half-gore model should provide a reasonable first approximation to the stress state of the balloon membrane away from these isolated regions. Using this information, one could then carry out a local analysis of high-stress regions.

IV. Conclusions

It is important to study the configuration of a balloon in the launch spool because this is when the maximum film stresses are likely to be experienced. We develop a mathematical model to estimate stresses in a nonfully deployed balloon with constraints, including a spool-like configuration. Large-scale features such as folds of excess material are represented explicitly through a virtual fold model. Small-scale features such as fine wrinkling are modeled by relaxation of the film strain energy density. For small volumes, such as those corresponding to a spool shape, the virtual fold model in conjunction with energy relaxation provides important information: estimates of the film stress resultants and an estimate of the distribution of folded material. We find that for a design shape representative of one used in scientific ballooning, the maximum film stresses at launch and in early stages of flight are nearly two and one-half times the magnitude of those computed for the float conditions. The external caps that serve to reinforce the balloon while being held in the launch spool, also serve to reinforce the balloon during the very early stages of ascent.

Acknowledgments

The research presented in this paper was supported by NASA Grant NAG5-697. Portions of this work were presented by the first author at the AIAA International Balloon Technology Conference, Norfolk, Virginia, June 1999.

References

[1]Baginski, F., and Brakke, K. A., "Modeling Ascent Configurations of Strained High-Altitude Balloons," *AIAA Journal*, Vol. 36, No. 10, 1998, pp. 1901–1910.

[2]Collier, W., "Estimating Stresses in a Partially Inflated High Altitude Balloon Using a Relaxed Energy Approach," *Quarterly of Applied Mathematics* (to be published).

[3]Baginski, F., "Modeling the Shapes of Constrained Partially Inflated High Altitude Balloons," AIAA Paper 99-3842, June 1999.

[4]Schrefler, B. A., and Contri, P., "A Geometrically Nonlinear Finite Element Analysis of Wrinkled Membrane Surfaces by a No-Compression Material Model," *Communications on Applied Numerical Methods*, Vol. 4, No. 1, 1988, pp. 5–15.

[5]Oden, J. T., *Finite Elements of Nonlinear Continua*, McGraw–Hill, New York, 1972, Chap. 18.

[6]Baginski, F., and Collier, W., "A Mathematical Model for the Strained Shape of a Large Scientific Balloon at Float Altitude," *Journal of Applied Mechanics,* Vol. 67, No. 1, 2000, pp. 6–16.

[7]"Research and Development in the Field of High Altitude Plastic Balloons," Dept. of Physics, Repts. NONR-710(01), Univ. of Minnesota, Minneapolis, MN, 1951–1956.

[8]Baginski, F., Collier, W., and Williams, T., "A Parallel Shooting Method for Determining the Natural-Shape of a Large Scientific Balloon," *SIAM Journal on Applied Mathematics*, Vol. 58, No. 3, 1998, pp. 961–974.

[9]Pipken, A. C., "Relaxed Energy Densities for Large Deformations of Membranes," *Journal of Applied Mathematics*, Vol. 52, 1994, pp. 297–308.
[10]Collier, W., "Applications of Variational Principles to Modeling a Partially Inflated Scientific Research Balloon," Ph.D. Thesis, Dept. of Mathematics, George Washington Univ., Washington, DC, Jan. 2000.
[11]Morris, A. L., (ed.), *Scientific Ballooning Handbook*, National Center for Atmospheric Research, NCAR-TN-99, Boulder, CO, 1975. Sec. V, pp. 1–45.
[12]Fisher, D., "Configuration Dependent Pressure Potentials," *Journal of Elasticity*, Vol. 19, 1988, pp. 77–84.
[13]Oden, J. T., and Carey, G. F., *Finite Elements. Special Problems in Solid Mechanics*, Vol. 5, Prentice–Hall, Englewood Cliffs, NJ, 1984, pp. 1–20.
[14]Antman, S. S., *Nonlinear Problems of Elasticity*, Springer-Verlag, New York, 1995, Chap. 12.
[15]Warren, J. C., Smalley, J. H., and Morris, A. L., "Aerostatic Lift of Helium and Hydrogen in the Atmosphere," National Center for Atmospheric Research, NCAR-TN/IA-69, Boulder, CO, Dec. 1971, p. 73.
[16]Schur, W., "Structural Behavior of Scientific Balloons; Finite Element Simulation and Verification," AIAA Paper 91-3668, 1991.
[17]Winker, J. A., "Stress Patterns, Shape Studies, and Failure Analysis on Real Balloons," AIAA Paper 86-2518, 1986.

S. Saigal
Associate Editor